Equal-interval splitting of quantum tunneling in single-molecule magnets with identical exchange coupling

Yan-Rong Li, Rui-Yuan Liu, Hai-Qing Liu, and Yun-Ping Wang
Beijing National Laboratory for Condensed Matter Physics, Institute of Physics, Chinese Academy of Sciences, Beijing 100190, People's Republic of China
(Received 22 January 2014; published 1 May 2014)

The equal-interval splitting of quantum tunneling observed in simple-Ising-model systems of Ni_4 (3D) and Mn_3 (2D) single-molecule magnets (SMMs) is reported. The splitting is due to the identical exchange coupling in the SMMs, and is simply determined by the difference between the two numbers of the spin-down $n_\downarrow$ and spin-up $n_\uparrow$ molecules neighboring to the tunneling molecule. The splitting may be presented as $(n_\downarrow - n_\uparrow)JS/g\mu_0\mu_B$, and the number of the splittings follows $n+1$ where $n = n_\downarrow + n_\uparrow$ is the coordination number. Besides, since the quantum tunneling is heavily dependent on local spin environment, the manipulation of quantum tunneling may become feasible for this kind of system, which may shed light on applications of SMMs.

DOI: 10.1103/PhysRevB.89.184401 PACS number(s): 75.45.+j, 75.50.Xx, 05.50.+q, 75.30.Et

Single-molecule magnets (SMMs) have been used as model systems to study the interface between classical and quantum behaviors, and are considered to be the most promising systems for the applications in quantum computing, high-density information storage, and magnetic refrigeration [1–5] due to the quantum tunneling of magnetization (QTM) observed in these systems [6–9]. Recent researches in the impact of intermolecular exchange couplings upon the QTM have focused on whether the exchange coupling may change the quantum tunneling in SMMs. The SMM dimer system is reported to have different quantum behavior from that of the individual SMMs, due to the intermolecular exchange couplings between the two components [10,11]. It is also reported that, in the SMM dimer with a three-dimensional (3D) network of exchange couplings, the QTM is not suppressed [12]. In this paper we demonstrate that, for the SMMs with identical exchange coupling (IEC), the quantum tunneling behavior is much simpler and the QTM might be conveniently manipulated by controlling of the magnetization.

In the following, we report a unique quantum tunneling effect observed in the single-molecule magnets of $[Ni(hmp)(CH_3CH_2OH)Cl]_4$ (hereafter Ni_4) [13,14] and $[Mn_3O(Et\text{-}sao)_3(MeOH)_3(ClO_4)]$ (hereafter Mn_3) [15,16]. The samples of Ni_4 and Mn_3 SMMs are prepared with the process reported in [13] and [15], respectively, and the quality of both samples are checked by using the four-circle diffractometer. The Ni_4 SMM is a crystal with a 3D network of exchange coupling, in which each molecule is coupled with four neighboring molecules by Cl$\cdots$Cl contact (which contributes to the exchange coupling) forming a diamondlike lattice. The Ni_4 crystal has S_4 symmetry, which ensures that the four exchange couplings between each molecule and its four neighboring molecules are identical throughout the crystal. The Mn_3 SMM is a crystal with a two-dimensional (2D) network of exchange coupling, in which each molecule is coupled with three neighboring molecules by hydrogen bonds (which contributes to the exchange coupling) in an ab plane, forming a honeycomblike structure viewed down along the c axis. The Mn_3 crystal has C_3 symmetry, which ensures that the three exchange couplings between each molecule and its three neighboring molecules are identical throughout the crystal. We notice that both Ni_4 and Mn_3 SMMs are crystals with IEC and the model systems of a simple Ising model [17]. We have observed the equal-interval splitting of quantum tunneling induced by IEC in these two systems by ac susceptibility and hysteresis loop measurements.

The blocking temperature of Ni_4 SMM is estimated to be 0.29 K according to the magnetic relaxation study [18], therefore we studied quantum tunneling effects of Ni_4 SMM by ac susceptibility measurements [19] instead of dc susceptibility measurements at temperatures above 0.5 K, with a homemade compensation measurement setup [18]. Figure 1 has demonstrated the temperature dependence of the quantum tunneling behavior in Ni_4 SMM, it is seen that the tunneling peaks appear with an equal interval. Apparently the peak at zero field disappears at 0.75 and 0.5 K, which consists of the missing step at zero field in magnetization hysteresis loops at 40 mK [13]. The shift of the tunneling peaks from higher to lower field with the increasing T is due to the enhancement of the effect of thermal activation upon tunneling [20,21]. We have also measured the quantum tunnelings at different orientations, and found the different resonant fields given in Ref. [13] are due to misalignment. Figure 2(a) demonstrates the field dependence of susceptibility at different given orientations. Note that the four peak positions in the red curve with $\theta = 43$ deg is in good agreement with the four step fields of -0.28, -0.15, 0.15, and 0.28 T of the hysteresis loops in Ref. [13], where the applied field is said to be parallel to the easy axis. It is worth mentioning that the easy axis of Ni_4 is very likely to get confused due to the irregular polyhedral shape of the sample. We have confirmed the easy axis by numerous tests, and the consistence of the resonant field component parallel to the easy axis for each orientation demonstrated in Fig. 2(b) suggests that the resonant fields along the easy axis of the sample are -0.21, -0.11, 0.11, and 0.21 T at 0.5 K.

The higher blocking temperature allows us to study the hysteresis loops above 1.6 K for Mn_3 SMM. Figure 3 shows the typical steplike hysteresis loops of Mn_3 SMM at different temperatures. The blocking temperature estimated from ZFC (zero field cooling) and FC (field cooling) curves shown in the inset is around 3 K. The sweep-rate-dependent magnetization curves at 1.6 K are shown in Fig. 4, with only a dM/dH curve at the sweeping rate of 0.0005 T/s presented for simplicity. A series of quantum tunneling peaks with an equal interval of

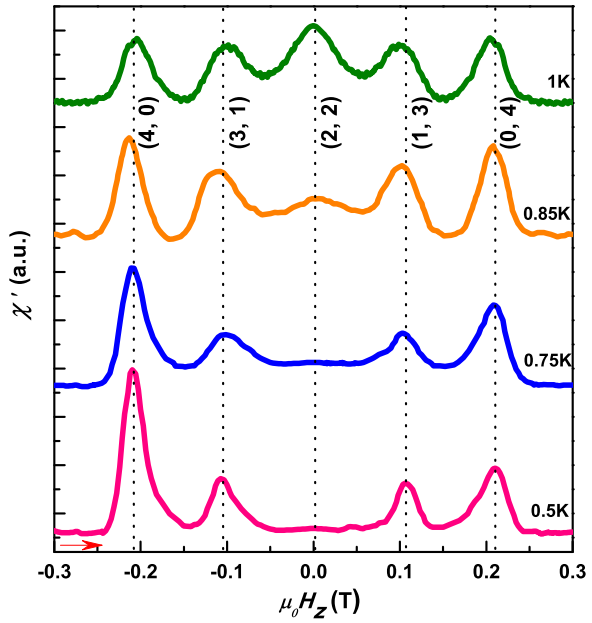

FIG. 1. (Color online) Field dependence of susceptibility χ' from -0.3 to 0.3 T at different temperatures measured on the Ni_4 single crystal, with the sweeping rate of 0.001 T/s and frequency of 11.3 kHz. The quantum tunneling peaks marked by black dotted lines originate from tunnelings between $|-4\rangle$ and $|4\rangle$ spin state, and the labeled number set in parentheses besides each dotted line indicates the local spin environment $(n_\downarrow, n_\uparrow)$ of the tunneling molecules.

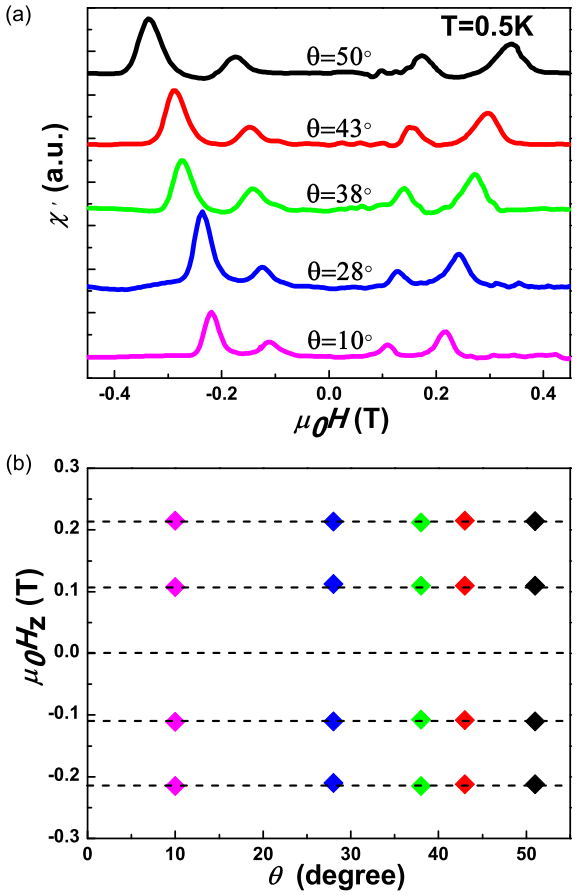

FIG. 2. (Color online) (a) Field dependence of susceptibility χ' from -0.45 to 0.45 T at different given orientations measured on the Ni_4 single crystal, with the sweeping rate of 0.001 T/s and frequency of 11.3 kHz. (b) The field component parallel to the easy axis vs the angle between the field direction and the easy axis. Each group of data with the same orientation is obtained from the corresponding resonant field on the χ'-H curves with the same color in (a).

0.36 T are observed in the dM/dH curves, which is similar to those observed in Ni_4 SMM.

Even though the influence of the intermolecular exchange interaction on the quantum tunnelings has been mentioned in the earlier literature [13,15], an unambiguous, systematical interpretation is badly needed to explain the quantum tunneling steps in Ni_4 and Mn_3 SMMs. With IEC taken into account, the molecules are not isolated, and the spin Hamiltonian of each molecule may be presented as

$$\hat{\mathcal{H}} = -D\hat{S}_z^2 + g\mu_0\mu_B\hat{S}_z H_z - \sum_{i=1}^{n} J\hat{S}_z\hat{S}_{iz} + \hat{\mathcal{H}}^{\text{trans}}, \qquad (1)$$

where D is the axial anisotropy constant, n is coordination number, J is the exchange interaction constant, $\hat{S}_z$ and $\hat{S}_{iz}$ are the easy-axis spin operators of the molecule and its ith exchange-coupled neighboring molecule, and $\hat{\mathcal{H}}^{\text{trans}}$ is the small off-diagonal perturbation term which comes from the transverse anisotropy induced by the finite-fold axial-rotation symmetry of the crystal, the transverse exchange coupling between the tunneling molecule and its neighboring molecules, and the transverse component of the effective magnetic field including classical dipolar magnetic field. $\hat{\mathcal{H}}^{\text{trans}}$ contributes to the quantum tunneling between level-crossing spin states and is negligible in calculating the energy of the spin states. For Ni_4, $S = 4$, $D = 0.86$ K, $g = 2.12$ [13,14]; while for Mn_3, $S = 6$, $D = 0.98$ K, $g = 2.06$ [16].

In Ni_4 SMM, every Ni_4 molecule has four AFM exchange-coupled neighboring molecules, and hence for each molecule there are five different kinds of local spin environment (LSE), which may be labeled by $(n_\downarrow, n_\uparrow)$, where $n_\downarrow$ and $n_\uparrow$ represent

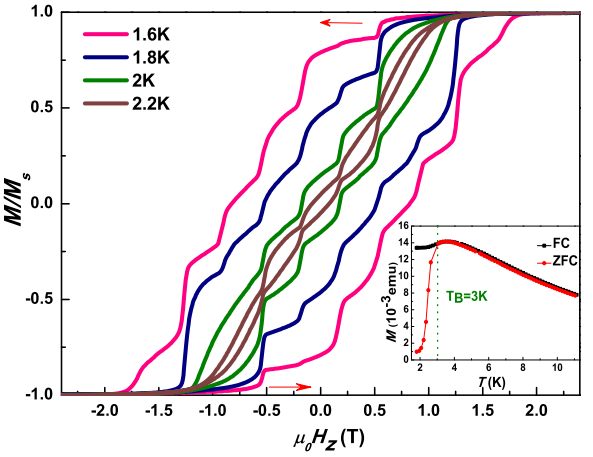

FIG. 3. (Color online) Magnetization (M/M_s) of Mn_3 single crystal versus applied magnetic field with the sweeping rate of 0.003 T/s at different temperatures. The inset shows ZFC and FC curves.

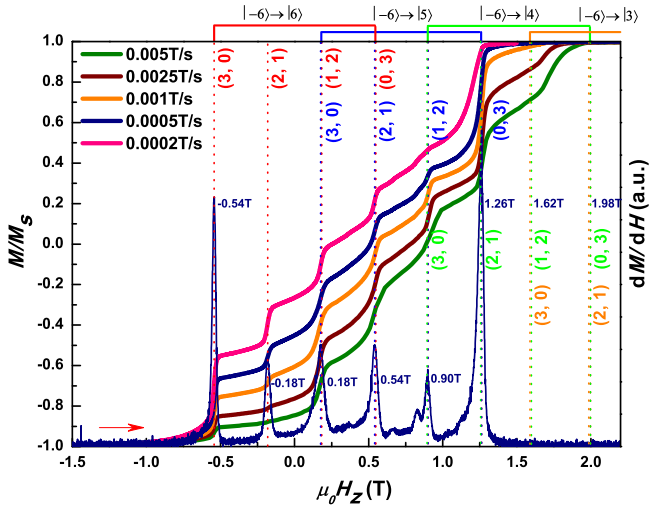

FIG. 4. (Color online) Sweep-rate-dependent magnetization (M/M_s) versus applied magnetic field $\mu_0 H_z$ (from −1.5 to 2.2 T) at 1.6 K measured on Mn_3 single crystal. The dM/dH curve with a sweeping rate of 0.0005 T/s is given. The quantum tunneling peaks marked by the dotted lines of the same color belong to the same tunneling of $|m_i\rangle \rightarrow |m_f\rangle$, the labeled number set in parentheses besides each dotted line indicates the local spin environment ($n_\downarrow$,$n_\uparrow$) of the tunneling molecules.

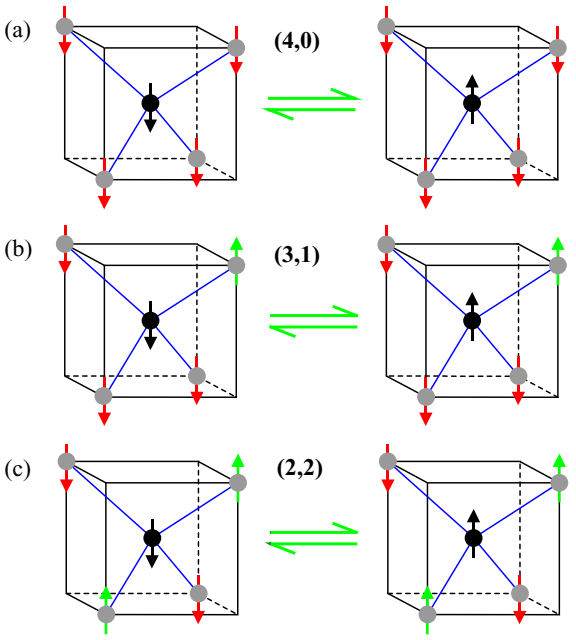

FIG. 5. (Color online) Sketch maps of three pairs of spin configurations with different LSE ($n_\downarrow$,$n_\uparrow$) in Ni_4 SMM, in correspondence to the tunnelings occurring at −0.21, −0.11, and 0 T in Fig. 1, respectively. Other equivalent spin configurations are not listed here for simplicity. The tunneling molecule is marked in black with a black arrow indicating its spin state, its four neighbors are marked in gray, with green and red arrows indicating spin-up and spin-down states, respectively, the blue lines between molecules represents the exchange couplings.

the number of the neighboring molecules which occupy $S_z = -4$ (hereafter $|-4\rangle$) and $S_z = 4$ (hereafter $|4\rangle$) spin states, respectively. (The excited spin states are not considered here, because most of them are not populated at our measurement temperatures.) At negative saturated field, all the molecules initially occupy $|-4\rangle$ in the same LSE (4,0) shown in Fig. 5(a) (left). According to Eq. (1), $|-4\rangle$ and $|4\rangle$ spin states in the LSE (4,0) are degenerate when the field reaches $4JS/g\mu_0\mu_B$, therefore those molecules which occupy the $|-4\rangle$ spin state in the LSE (4, 0) [Fig. 5(a)] have the same probability to undergo tunneling at $4JS/g\mu_0\mu_B$, leading to the resonant tunneling peaks at −0.21 T as seen in Fig. 1. Following this resonant quantum tunneling, some molecules will occupy $|4\rangle$ spin state, and the LSE of the molecules will not be identical any more. When the field reaches $2JS/g\mu_0\mu_B$ (corresponding to −0.11 T as seen in Fig. 1), the resonant tunneling takes place from $|-4\rangle$ to $|4\rangle$ spin state in the LSE (3, 1) [Fig. 5(b)]. As a matter of fact, at zero field the tunneling of the molecules in the LSE (2, 2) [Fig. 5(c)] will change neither Zeeman energy nor the exchange interaction energy, which gives rise to the macroscopic quantum tunneling observed at zero field at relatively higher temperatures shown in Fig. 1. Similarly, there are quantum tunnelings taking placing from $|-4\rangle$ to $|4\rangle$ spin state with the LSE (1, 3) at $-2JS/g\mu_0\mu_B$, and from $|-4\rangle$ to $|4\rangle$ spin state with the LSE (0, 4) at $-4JS/g\mu_0\mu_B$. The exchange interaction constant J is calculated to be −0.019 K according to the splitting interval, which is close to the simulation value −0.02 K obtained from the experimental AFM transition temperature of $T_N = 0.91$ K [22]. For Ni_4 SMM, the system enters into a long-range AFM order at 0.91 K [22] instead of being frozen below the blocking temperature, therefore at temperatures obviously below T_N, the spins of the molecules will be antiparallel to its neighbors, i.e., the molecules are in the LSE (0, 4) and (4, 0) instead of the LSE (2, 2), which causes the missing of quantum tunneling at zero field at $T \leqslant 0.75$ K as seen in Fig. 1. However, in the vicinity of the transition temperature, some molecules are still in the LSE (2, 2) due to the thermal fluctuation, thus there is still evidence of resonant quantum tunneling at 0.85 K at zero field shown in Fig. 1.

Mn_3 SMM displays a finer quantum tunneling behavior than Ni_4 SMM. Every Mn_3 molecule has three AFM exchange-coupled neighboring molecules, and hence for each molecule there are four different kinds of local spin environment as shown in Fig. 6, labeled as (3, 0), (2, 1), (1, 2), and (0, 3), respectively, thus there are quantum tunnelings occurring at $3JS/g\mu_0\mu_B$, $JS/g\mu_0\mu_B$, $-JS/g\mu_0\mu_B$, and $-3JS/g\mu_0\mu_B$ from $|-6\rangle$ to $|6\rangle$ spin state, which is corresponding to the four tunneling peaks marked by the red dotted lines shown in Fig. 4.

In both Mn_3 and Ni_4 SMMs, with the presence of IEC, the tunneling between two ground spin states of $|\pm S\rangle$ is split by an equal-interval field of $2|J|S/g\mu_0\mu_B$. Generally, according to Eq. (1), the tunneling from $|-S\rangle$ to $|S-l\rangle$ is split by the same equal-interval field, and the split tunneling field may be simply expressed as

$$H_z = lD/g\mu_0\mu_B + (n_\downarrow - n_\uparrow)JS/g\mu_0\mu_B. \qquad (2)$$

The first term comes from the internal spin states in each molecule, and the second term is of the tunneling splitting induced by IEC. The splitting is simply determined by the difference between the two numbers of the spin-down ($n_\downarrow$) and spin-up ($n_\uparrow$) molecules neighboring to the tunneling

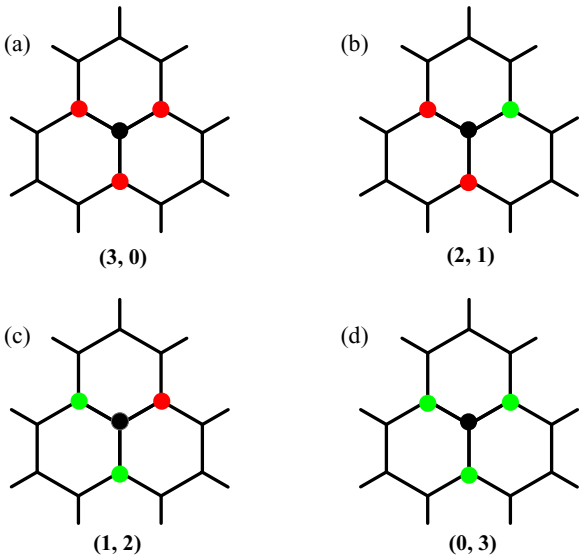

FIG. 6. (Color online) Sketch maps of four spin configurations with different LSE $(n_\downarrow,n_\uparrow)$ in Mn_3 SMM, other equivalent spin configurations are not listed here for simplicity. The tunneling molecule is marked in black, which could occupy either a spin-up or spin-down state. Its neighboring molecules occupying spin-up and spin-down states are marked in green and red, respectively. The black lines between molecules represent the exchange couplings.

molecule. According to Eq. (2), the number of splittings equals the number of different kinds of $(n_\downarrow, n_\uparrow)$ LSEs, and hence may be expressed as $\binom{n+1}{1} = n+1$ by combinatorics, where $n = n_\downarrow + n_\uparrow$.

According to Eq. (2), when $D > n|J|S$ and $|H_z| < (D - n|J|S)/g\mu_0\mu_B$, any quantum tunneling with $l \neq 0$ are not allowed; while according to Eq. (1), when the first excitation energy of a molecule $D(2S-1) \gg kT$, almost all molecules will occupy the two ground spin states of $|\pm S\rangle$. Therefore, under the above conditions, Eq. (1) may be simplified as

$$\hat{\mathcal{H}} = g\mu_0\mu_B \hat{S}_z H_z - \sum_{i=1}^{n} J \hat{S}_z \hat{S}_{iz}, \tag{3}$$

which is just the Hamiltonian of simple Ising model [17]. For both Ni_4 and Mn_3, $D > n|J|S$, thus Ni_4 and Mn_3 SMMs are good model systems of a simple Ising model at low temperature and low field, which are important for the studies of quantum tunneling behavior and related applications.

Since the intermolecular exchange couplings are identical in the system, the magnitude $\mathcal{T}$ of a tunneling may be simply factorized into intermolecular contribution $N_{(n_\downarrow,n_\uparrow)}$ and intramolecular contribution $P_{|m_i\rangle\to|m_f\rangle}$,

$$\mathcal{T} = \alpha N_{(n_\downarrow,n_\uparrow)} P_{|m_i\rangle\to|m_f\rangle}, \tag{4}$$

where $N_{(n_\downarrow,n_\uparrow)}$ is the number of molecules with the LSE $(n_\downarrow,n_\uparrow)$, $P_{|m_i\rangle\to|m_f\rangle}$ is the tunneling probability of the molecule from the spin state $|m_i\rangle$ to $|m_f\rangle$, and α is a constant. $N_{(n_\downarrow,n_\uparrow)}$ strongly depends on the magnetization M and may be easily modulated, while $P_{|m_i\rangle\to|m_f\rangle}$ is determined by the tunneling barrier between $|m_i\rangle$ and $|m_f\rangle$ inside molecules and is hardly to be controlled. Therefore, for SMMs-with-IEC, with the dependence of $\mathcal{T}$ on $N_{(n_\downarrow,n_\uparrow)}$, the manipulation of quantum tunneling should be rather simple.

The quantum tunnelings from the same initial states $|m_i\rangle$ to the same final states $|m_f\rangle$ but with different LSEs are referred to as a tunneling set. The five tunneling peaks of Ni_4 SMM in Fig. 1 belong to the same set of $|-4\rangle \to |4\rangle$ and has the same $P_{|m_i\rangle\to|m_f\rangle}$, thus the intensities of the five peaks is proportional to $N_{(n_\downarrow,n_\uparrow)}$, which means that $N_{(n_\downarrow,n_\uparrow)}$ may be monitored by macroscopic measurements of the tunneling peaks. For Mn_3 SMM, the AFM exchange coupling constant J is calculated to be $J = -0.041$ K according to the field interval of the $|-6\rangle \to |6\rangle$ tunneling set (Fig. 4). However, the axial anisotropy constant $D = 0.98$ K [16] of Mn_3 SMM happens to be close to $4|J|S$, which results in the overlap of two adjacent tunneling sets demonstrated by the overlapped dotted lines shown in Fig. 4. The tunneling steps at 0.18 and 0.54 T are the combinations of the tunnelings from $|-6\rangle$ to $|6\rangle$ spin state with the LSEs (1, 2) and (0, 3) (marked by red dotted lines) and quantum tunnelings from $|-6\rangle$ to $|5\rangle$ spin state with the LSEs (3, 0) and (2, 1) (marked by blue dotted lines), respectively. Similarly, all subsequent tunneling steps are combinations of quantum tunnelings in different tunneling sets with different local spin environments. It may be worth a mention that the tunnelings are expected to occur at 1.62 and 1.98 T (marked by green and orange dotted lines) at lower temperatures as well, although not observed in these curves.

Of the overlapped tunnelings mentioned above, due to the dependence of tunneling on the local spin environment, the contribution of the individual tunneling changes as the field sweeping rate varies. For example, the tunneling step at 0.18 T is the combination of tunneling from $|-6\rangle$ to $|6\rangle$ spin state with the LSE (1, 2) and tunneling from $|-6\rangle$ to $|5\rangle$ spin state with the LSE (3, 0), therefore the tunneling magnitude is determined by $N_{(3,0)}P_{|-6\rangle\to|5\rangle} + N_{(1,2)}P_{|-6\rangle\to|6\rangle}$, where $N_{(3,0)}$ and $N_{(1,2)}$ strongly depends on the magnetization M. As shown in Fig. 4, for the tunneling at 0.18 T, M/M_s is increasing with the decreasing of field sweeping rate, which suggests that $N_{(1,2)}$ is increasing while $N_{(3,0)}$ is decreasing, and hence the contribution of the tunneling from $|-6\rangle$ to $|6\rangle$ spin state with the LSE (1, 2) is taking the dominance from the contribution of the tunneling from $|-6\rangle$ to $|5\rangle$ spin state with the LSE (3, 0), eventually.

Due to the strong dependency of a tunneling on the $N_{(n_\downarrow,n_\uparrow)}$ based on Eq. (4), the subsequent quantum tunneling heavily depends on the the preceding quantum tunnelings in SMMs-with-IEC. As shown in Fig. 4, tunneling at -0.54 T [from $|-6\rangle$ to $|6\rangle$ spin state with the LSE (3, 0)] is inherited by tunneling at -0.18 T [from $|-6\rangle$ to $|6\rangle$ spin state with the LSE (2, 1)], the tunnelings at -0.54, -0.18 T are further carried on by the next tunneling, and the process continues as the LSE changes. In fact, the history dependence is not prominent for Ni_4 SMM, due to that the measurements were performed at temperatures much higher than its blocking temperature, while thermal activated effect ruins the memory of history. Apparently the subsequent quantum tunneling is more heavily dependent on the preceding quantum tunnelings in SMMs-with-IEC when the thermal activated effect is severely suppressed as the temperature drops adequately. This indicates a way for manipulating quantum tunneling.

In summary, we performed detailed ac susceptibility and hysteresis loop measurements on Ni_4 and Mn_3 single crystals, respectively, and have observed the equal-interval splitting of quantum tunneling in both systems, the splitting of quantum tunneling is presented by $(n_\downarrow - n_\uparrow)JS/g\mu_0\mu_B$; and the number of splitting follows $n+1$, where $n = n_\downarrow + n_\uparrow$ is the coordination number. Since the splitting is induced by the IEC between the molecules, the rules should be universally applicable to all single-molecule magnets with IEC. Besides, it is demonstrated that the manipulation of quantum tunneling may become feasible for this kind of system, which may shed light on applications of SMMs.

Compared to the earlier researches, the identical exchange coupling (IEC) is underlined in our study. Earlier models are based on the dimer systems without IEC, in which the quantum behaviors are much more complicated because: (1) there might be hundreds or even thousands of possible different resonant fields while a hundred energy states are allowed in the dimer system [10]; and (2) the exchange interaction J' between two dimers are not negligible, and should be considered in addition to the exchange interaction J between the two component units within a dimer, which has greatly added the complexity of the quantum tunneling [11,12]. However, Ni_4 and Mn_3 with IEC are not dimer systems, and therefore the models for the dimer systems are not applicable. The presence of IEC in both Ni_4 and Mn_3 SMM is of distinct importance, because the network of IEC across the system resulted in: (1) the number of possible resonant fields is tremendously reduced by degeneracy of the energy states which is manifested with the equal-interval splitting observed; and (2) a universally applicable exchange interaction J between any two coupled molecules within the IEC network is taking over the two different types of exchange interactions J and J' in the dimer system. Therefore, the picture of the quantum behaviors in the SMMs with IEC is much more simplified. Apparently the simplicity of the picture is of great significance in helping to understand the quantum tunneling behaviors as well as to inspire the applications.

We thank Professor Dianlin Zhang, Lu Yu, and Li Lu for helpful discussions. We also thank Shaokui Su for experimental assistance. This work was supported by the National Key Basic Research Program of China (No. 2011CB921702) and the Natural Science Foundation of China (No. 11104331).

[1] M. N. Leuenberger and D. Loss, Nature (London) **410**, 789 (2001).
[2] J. Tejada, E. M. Chudnovsky, E. del Barco, J. M. Hernandez, and T. P. Spiller, Nanotechnology **12**, 181 (2001).
[3] L. Bogani and W. Wernsdorfer, Nat. Mater. **7**, 179 (2008).
[4] J. Tejada, Polyhedron **20**, 1751 (2001).
[5] F. Torres, J. M. Hernandez, X. Bohigas, and J. Tejada, Appl. Phys. Lett. **77**, 3248 (2000).
[6] J. R. Friedman, M. P. Sarachik, J. Tejada, and R. Ziolo, Phys. Rev. Lett. **76**, 3830 (1996).
[7] L. Thomas, F. Lionti, R. Ballou, D. Gatteschi, R. Sessoli, and B. Barbara, Nature (London) **383**, 145 (1996).
[8] C. Sangregorio, T. Ohm, C. Paulsen, R. Sessoli, and D. Gatteschi, Phys. Rev. Lett. **78**, 4645 (1997).
[9] K. L. Taft, C. D. Delfs, G. C. Papaefthymiou, S. Foner, D. Gatteschi, and S. J. Lippard, J. Am. Chem. Soc. **116**, 823 (1994).
[10] W. Wernsdorfer, N. Aliaga-Alcalde, D. N. Hendrickson, and G. Christou, Nature (London) **416**, 406 (2002).
[11] W. Wernsdorfer, S. Bhaduri, R. Tiron, D. N. Hendrickson, and G. Christou, Phys. Rev. Lett. **89**, 197201 (2002).
[12] R. Tiron, W. Wernsdorfer, N. Aliaga-Alcalde, and G. Christou, Phys. Rev. B **68**, 140407(R) (2003).
[13] E. C. Yang *et al.*, Polyhedron **22**, 1727 (2003).
[14] E. C. Yang *et al.*, Inorg. Chem. **45**, 529 (2006).
[15] R. Inglis, L. F. Jones, G. Karotsis, A. Collins, S. Parsons, S. P. Perlepes, W. Wernsdorfer, and E. K. Brechin, Chem. Commun., 5924 (2008).
[16] R. Inglis, S. M. Taylor, L. F. Jones, G. S. Papaefstathiou, S. P. Perlepes, S. Datta, S. Hill, W. Wernsdorfer, and E. K. Brechin, Dalton Trans., 9157 (2009).
[17] H. A. Kramers and G. H. Wannier, Phys. Rev. **60**, 252 (1941).
[18] Y. R. Li, H. Q. Liu, Y. Liu, S. K. Su, and Y. P. Wang, Chin. Phys. Lett. **26**, 077504 (2009).
[19] F. Luis, J. Bartolome, J. F. Fernandez, J. Tejada, J. M. Hernandez, X. X. Zhang, and R. Ziolo, Phys. Rev. B **55**, 11448 (1997).
[20] L. Bokacheva, A. D. Kent, and M. A. Walters, Phys. Rev. Lett. **85**, 4803 (2000).
[21] J. J. Henderson, C. Koo, P. L. Feng, E. del Barcoxs, S. Hill, I. S. Tupitsyn, P. C. E. Stamp, and D. N. Hendrickson, Phys. Rev. Lett. **103**, 017202 (2009).
[22] J. W. Zuo, H. Q. Liu, Y. R. Li, S. K. Su, and Y. P. Wang, Sci. China-Phys. Mech. Astron. **55**, 11 (2012).